Molecular Crystals and Liquid Crystals Science and Technology. Section A. Molecular Crystals and Liquid Crystals

Publication details, including instructions for authors and subscription information:
http://www.tandfonline.com/loi/gmcl19

Orientational Order in the Smectic F and G Phases: Deuterium Nuclear Magnetic Resonance (NMR) Study

J. L. Figueirinhas [a] & J. W. Doane [b]

[a] Centro de Fisica da Materia Condensada, Av. Prof. Gama Pinto N°2, 1699, Lisboa Codex, Portugal

[b] Liquid Ctystal Institute, Kent State University, Kent, OH, 44242, USA

Version of record first published: 04 Oct 2006.

To cite this article: J. L. Figueirinhas & J. W. Doane (1994): Orientational Order in the Smectic F and G Phases: Deuterium Nuclear Magnetic Resonance (NMR) Study, Molecular Crystals and Liquid Crystals Science and Technology. Section A. Molecular Crystals and Liquid Crystals, 238:1, 61-81

To link to this article: http://dx.doi.org/10.1080/10587259408046916

Mol. Cryst. Liq. Cryst., 1994, Vol. 238, pp. 61–81
Reprints available directly from the publisher
Photocopying permitted by license only

Printed in the United States of America

Orientational Order in the Smectic F and G Phases: Deuterium Nuclear Magnetic Resonance (NMR) Study

J. L. FIGUEIRINHAS

Centro de Fisica da Materia Condensada, Av. Prof. Gama Pinto N°2, 1699 Lisboa Codex, Portugal

and

J. W. DOANE

Liquid Crystal Institute, Kent State University, Kent, OH 44242 USA

(Received February 15, 1993)

A deuterium NMR investigation of molecular orientational order in the hexatic S_F phase and the crystalline S_G phases exhibited by three liquid crystalline mixtures is described. Two homologues of the terephthal-bis-*n*-alkylanilines series were used; TBOA and TBDA in mixtures with TBBA. The principal values and orientation of the principal axes of the averaged electric field gradient (EFG) tensors from deuterated sites in the core and chain regions of the molecule were determined using both aligned (monodomain) and powder samples. It was found in both phases that the averaged EFG tensors from different deuterated sites in the molecule show different asymmetries and do not share the same principal axes. While the averaged EFG tensor from the alpha deuterated positions shows a near zero asymmetry parameter implying no in-plane order, the averaged EFG tensors from the core are strongly asymmetric indicating the existence of in-plane order. The values of the averaged EFG tensors show no discontinuity at the S_F-S_G phase transition. This implies the existence of local herringbone order in the S_F phase for the molecular core since this type of ordering is known to be present in the S_G phase. From the measured values of the EFG tensors of the molecular core the order of this part of the molecule is estimated in the context of a simple model describing its motions.

Keywords: smectic F, smectic G, NMR

I. INTRODUCTION

Since its discovery[1] the S_F phase was subjected to an intense investigation mainly by x-ray techniques.[2–10] The interest in this phase arose because it was claimed as a candidate for the stacked hexatic phase predicted in bulk liquid crystals by Birgeneau and Litster.[11] The hexatic phase was introduced as the bulk analog of the intermediate phase in the two-dimensional melting theory by Halperin and Nelson.[12] X-ray studies performed on this phase[3–10] yielded its structural properties including the molecular positional order, identifying the S_F phase as a stacked hexatic. A stacked hexatic phase is characterized by short-range positional order

in the layers, long range bond-orientational order and weak inter-layer coupling. In the tilted phases the direction of tilt is long range and is coupled to the bond-orientational order.[11] X-ray studies of the S_F phase by F. Moussa *et al.*[10] have identified the presence of two sub-layers, one formed by the aliphatic chains showing no in-plane order and other formed by the aromatic cores responsible for the molecular order. While positional order is well characterized in the S_F phase, orientational order in this phase has not been analyzed in complete detail.[13,14] The knowledge of the type of local molecular motion is important for phase characterization. In particular, the presence of local herringbone order already shown for the S_F phase of 90.4[14] is of theoretical importance since herringbone order is a relevant degree of freedom.[15] A deuterium NMR study can bring insight into local molecular motion by measuring molecular orientational order and determining in this way the presence of herringbone order.

II. THEORY

A. Theoretical Spectral Patterns

The spin Hamiltonian for deuterium in a magnetic field is[16]:

$$\mathbb{H} = \mathbb{H}_Z + \mathbb{H}_Q = -\gamma\hbar\mathbf{H}\cdot\mathbf{I} - \frac{1}{6}\sum Q_{ij}V_{ij} \tag{1}$$

where $\mathbb{H}_Z$ and $\mathbb{H}_Q$ are the Zeeman and quadrupolar interaction Hamiltonians. In liquid crystalline mesophases the molecules are undergoing rapid rotational and translational diffusion motions and the Quadrupolar interaction Hamiltonian becomes time averaged. In high field $\overline{\mathbb{H}_Q}$ can be treated in first order perturbation and this Hamiltonian yields an absorption spectra with two lines and a splitting between them given by:

$$\nu = \left|\frac{3}{2}\bar{v}_Q\left[P_2(\cos\theta) + \frac{\bar{\eta}}{2}\sin^2\theta\cos 2\phi\right]\right| \tag{2}$$

where θ and ϕ are the polar and azimuthal angles that give the orientation of the external magnetic field in the principal frame of the time averaged EFG tensor $\bar{V}_{ij}$. $\bar{v}_Q = (eQ/h)\bar{V}_{zz}$ is the time averaged quadrupolar coupling constant and $\bar{\eta} = (\bar{V}_{xx} - \bar{V}_{yy})/\bar{V}_{zz}$ is the time averaged asymmetry parameter.

To determine $\bar{v}_Q$ and $\bar{\eta}$ either aligned (monodomain) or powder samples can be used. From an aligned sample study it is also possible to determine the average molecular orientation in the smectic layers as shown below.

In a random powder sample, domains with all possible orientations relative to the external magnetic field are present. The absorption spectra of such a system can be calculated using Equation (2) assuming that the magnetic field is uniformly

distributed in space, which means that all values of θ and ϕ are equally present. The absorption spectra $G(\Omega)$ is:

$$G(\Omega) = \left|\frac{dN}{d\Omega}\right| = \int g(\Omega, \phi)\, d\phi \tag{3}$$

with $g(\Omega, \phi) = \left|\frac{dN}{d\Omega}\right|_\phi = \left|\frac{dN}{d\theta}\right|_\phi \left|\frac{d\theta}{d\Omega}\right|_\phi$, $\left|\frac{dN}{d\theta}\right|_\phi = C \sin\theta$.

The quantity $\left|\frac{d\theta}{d\Omega}\right|$ is evaluated from Equation (2). $G(\Omega)$ is finally given by:

$$G(\Omega) = \int_{\phi^-}^{\frac{\pi}{2}} \frac{8C}{3\pi\bar{\nu}_Q} \frac{d\phi}{\sqrt{(3 - \bar{\eta}\cos 2\phi)^2 - 2(3 - \bar{\eta}\cos 2\phi)\left(1 - \frac{2\Omega}{3\pi\bar{\nu}_Q}\right)}}\Bigg|_{-\frac{3\pi}{4}\bar{\nu}_Q(\bar{\eta}+1)\leq\Omega\leq\frac{3\pi}{2}\bar{\nu}_Q}$$

$$+ \int_{\phi^-}^{\frac{\pi}{2}} \frac{8C}{3\pi\bar{\nu}_Q} \frac{d\phi}{\sqrt{(3 - \bar{\eta}\cos 2\phi)^2 - 2(3 - \bar{\eta}\cos 2\phi)\left(1 + \frac{2\Omega}{3\pi\bar{\nu}_Q}\right)}}\Bigg|_{\frac{3\pi}{4}\bar{\nu}_Q(\bar{\eta}+1)\geq\Omega\geq-\frac{3\pi}{2}\bar{\nu}_Q} \tag{4}$$

with $\phi^\pm = \frac{1}{2}\arccos\left[\frac{1}{\bar{\eta}}\left(1 \pm \frac{4\Omega}{3\pi\bar{\nu}_Q}\right)\right]$.

The convolution of this function either with a Lorentzian or Gaussian line shapes gives broadening to the resonance lines from the residual dipolar interactions. Fitting $G(\Omega)$ to the experimental spectra yields $\bar{\nu}_Q$ and $\bar{\eta}$.

In a monodomain sample the absorption spectra is composed of two lines whose splitting is governed by Equation (2). To determine the principal values and orientation of the principal axes of the averaged EFG tensor it is nevertheless convenient to introduce an intermediate reference frame with its x,y plane parallel to smectic layers and the y axis coinciding with the sample rotation axis orthogonal to the magnetic field. (Figure 1) The quadrupolar splitting is given in this case by[14]:

$$\nu = |A_0 + A_1 \cos 2\theta_0 + B_1 \sin 2\theta_0| \tag{5}$$

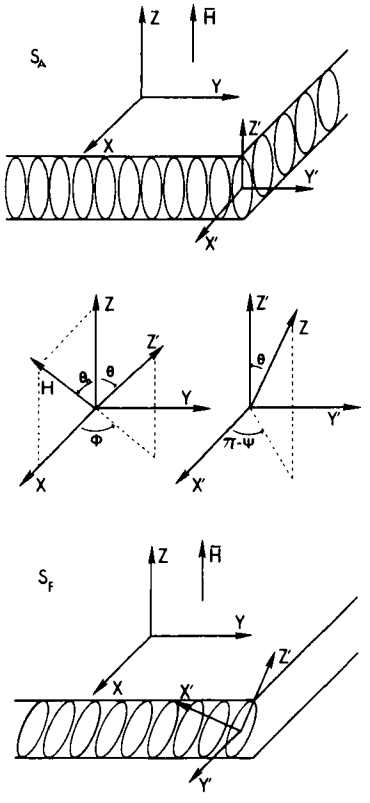

FIGURE 1 Illustration of the relationship between the sample frame (x, y, z) and the principal axes frame (x', y', z') for field aligned smectic layers. The Euler angles (ϕ, θ, ψ) and the magnetic field orientation (θ_0) are also shown.

with A_0, A_1 and B_1

$$A_0 = \frac{3}{8}\bar{v}_Q\left[\frac{1}{2}(3\cos^2\theta - 1 + \bar{\eta}\sin^2\theta\cos 2\psi) + \frac{3}{2}\sin^2\theta\cos 2\phi + \frac{\bar{\eta}}{2}((1 + \cos^2\theta)\cos 2\psi\cos 2\phi - 2\cos\theta\sin 2\psi\sin 2\phi)\right] \quad (6)$$

$$A_1 = \frac{3}{8}\bar{v}_Q\left[\frac{3}{2}(3\cos^2\theta - 1 + \bar{\eta}\sin^2\theta\cos 2\psi) - \frac{1}{2}[3\sin^2\theta\cos 2\phi + \bar{\eta}((1 + \cos^2\theta)\cos 2\psi\cos 2\phi - 2\cos\theta\sin 2\psi\sin 2\phi)]\right] \quad (7)$$

$$B_1 = \frac{3}{8}\bar{v}_Q[3\sin 2\theta\cos\phi - \bar{\eta}(\sin 2\theta\cos 2\psi\cos\phi - 2\sin\theta\sin 2\psi\sin\phi)] \quad (8)$$

The values of A_0, A_1 and B_1 are obtained by fitting the experimental splittings at different angles θ_0 to Equation (5) with a least squares routine. From these values it is possible to obtain the values of $\bar{v}_Q$, $\bar{\eta}$ and θ, solving the system of Equations (6), (7) and (8) where ψ is zero and ϕ is set either to zero or π. The value of ψ is imposed by the C_{2h} symmetry of the S_F and S_G phases.[17] The angle ϕ gives the tilt direction in the smectic planes. We are able to set it at zero or π because in the S_F aligned sample the molecules are seen to choose the orientation that minimizes the angle between the magnetic field and the principal z axes of the averaged EFG tensors which are close to the long molecular axis. In this way ϕ is automatically set either to zero or π.[14]

B. Order Parameters of the Molecular Core

The measured values of the averaged EFG tensors from the molecular core can yield quantitative information on the core order, when reasonable hypotheses regarding the motions involved are taken into account. The approach followed here generalizes those introduced in References 18–23. Both the principal values and orientation of the principal axes of the averaged EFG tensors from two distinct deuterated sites are simultaneously used in the model as wasn't done before. The averaged EFG tensors in the phase fixed frame of reference are related to their value in the average molecular frame through the superordering matrix S_{kl}^{ij}.[24] The lower indices refer to the phase fixed frame while the upper indices refer to the average molecular frame.

$$\bar{V}_{ij} = \left(\frac{2}{3} S_{ij}^{kl} + \frac{1}{3} \delta_{ij}\delta_{kl}\right) V_{kl} \tag{9}$$

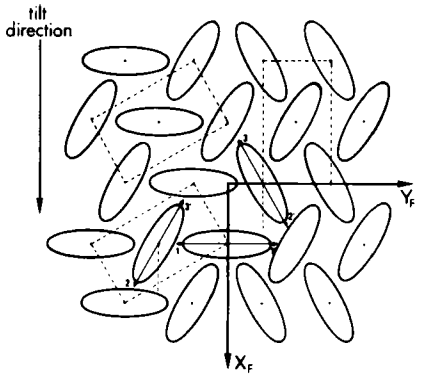

FIGURE 2 In plane structure present in a smectic phase when there is local herringbone order. 1, 1′, 2, 2′, 3, and 3′ are the possible orientations of the short molecular Y_M axis. Because of translational and rotational diffusion, in a time short compared to the NMR measurement time each molecule will sample all three possible orientations with different probabilities.

With a suitable choice of the phase frame, and due to the C_{2h} symmetry of the phases under study, the 25 independent elements of S, can be reduced to only 15 nonzero elements, yielding:

$$\begin{aligned} \tilde{V}_{ij} &= \left(\frac{2}{3} S_{ij}^{kl} + \frac{1}{3}\delta_{ij}\delta_{kl}\right) V_{kl}; \qquad \text{for } ij = xx, yy, zz, xz \\ \tilde{V}_{ij} &= 0; \qquad \text{for any other combination of } ij \end{aligned} \tag{10}$$

The orientation in the molecule of the principal molecular frame of S_{zz}^{kl} can be estimated with good approximation.[22] In this frame $\tilde{V}_{ij}$ is given by:

$$\begin{aligned} \tilde{V}_{zz} &= S_{zz}^{zz} V_{zz} + \frac{1}{3}(S_{zz}^{xx} - S_{zz}^{yy})(V_{xx} - V_{yy}) \\ \tilde{V}_{xx} - \tilde{V}_{yy} &= (S_{xx}^{zz} - S_{yy}^{zz})V_{zz} + \frac{1}{3}[(S_{xx}^{xx} - S_{yy}^{xx}) \\ &\quad - (S_{xx}^{yy} - S_{yy}^{yy})](V_{xx} - V_{yy}) \\ &\quad + \frac{4}{3}[(S_{xx}^{xy} - S_{yy}^{xy})V_{xy} + (S_{xx}^{xz} - S_{yy}^{xz})V_{xz} + (S_{xx}^{yz} - S_{yy}^{yz})V_{yz}] \\ \tilde{V}_{xz} &= S_{xz}^{zz} V_{zz} + \frac{1}{3}(S_{xz}^{xx} - S_{xz}^{yy})(V_{xx} - V_{yy}) \\ &\quad + \frac{4}{3}[S_{xz}^{xy} V_{xy} + S_{xz}^{xz} V_{xz} + S_{xz}^{yz} V_{yz}] \end{aligned} \tag{11}$$

The large quadrupolar splittings obtained experimentally both in the S_F and S_G phases indicate that orientational order should be high in these phases. Molecular motions in the herringbone lattice are then mainly rotational motions around the long molecular axis and diffusional jumps between the different sites in the lattice. This motion causes the short molecular axes to assume the three types of orientations shown in Figure 2. The order parameters will depend primarily upon the probabilities of occupation of the different orientations and on the librations around those orientations. The long molecular axis is taken to fluctuate in an unbiased fashion around its equilibrium orientation. This will exclude the possible contribution of biased fluctuations of this axis for the asymmetry in $\tilde{V}_{ij}$. Nevertheless this contribution is small since the asymmetry in $\tilde{V}_{ij}$ is highly temperature dependent while the long axis order is not. The presence of noticeable temperature dependent

biased fluctuations of the long axis, will cause a temperature dependent long axis order. Under the previous considerations, $\bar{V}_{ij}$ is given by:

$$\bar{V}_{zz} = S_{zz}^{zz} V_{zz}$$

$$\bar{V}_{xx} - \bar{V}_{yy} = \frac{1}{3}[(S_{xx}^{xx} - S_{yy}^{xx}) - (S_{xx}^{yy} - S_{yy}^{yy})](V_{xx} - V_{yy}) \tag{12}$$

$$\bar{V}_{xz} = \frac{4}{3} S_{xz}^{yz} V_{yz}$$

The EFG tensor V_{ij} in the molecular frame is obtained averaging the EFG from the deuterated positions over the motions around the preferred conformation of the molecular core taken to be all-trans. These motions are modeled assuming the existence of a hindering potential of the type $V_0 \cos(2\phi)$ whose strength V_0 is a fitting parameter. The phenyl rings are assumed to be executing π flips and small vibrations around a preferred orientation in the molecular frame. The amplitude of the small ring vibrations and its preferred orientation appear coupled in this model and are given by the parameter ξ. To end the description of the model we must relate the quantities $\bar{V}_{ij}$ to the values measured in the laboratory. This is achieved by rotating the measured EFG tensors from their principal frames to the phase frame around the C_2 symmetry axis. This rotation involves the rotation angle ε which is the third fitting parameter in the model. The values of V_0, ξ and ε are found solving the set of equations:

$$\frac{\bar{V}_{zz}^r}{V_{zz}^r} = \frac{\bar{V}_{zz}^m}{V_{zz}^m}, \quad \frac{\bar{V}_{xx}^r - \bar{V}_{yy}^r}{V_{xx}^r - V_{yy}^r} = \frac{\bar{V}_{xx}^m - \bar{V}_{yy}^m}{V_{xx}^m - V_{yy}^m}, \quad \frac{\bar{V}_{xz}^r}{V_{yz}^r} = \frac{\bar{V}_{xz}^m}{V_{yz}^m} \tag{13}$$

The different V_{ij} are given in frequency units by:

$$\bar{V}_{zz}^r = \bar{v}_Q^r \left\{ \frac{3}{2} \cos^2(\varepsilon + t) - \frac{1}{2} + \frac{\bar{\eta}^r}{2} \sin^2(\varepsilon + t) \right\}$$

$$\cdot \bar{V}_{zz}^m = \bar{v}_Q^m \left\{ \frac{3}{2} \cos^2\varepsilon - \frac{1}{2} + \frac{\bar{\eta}^m}{2} \sin^2\varepsilon \right\}$$

$$V_{zz}^r = v_Q^r \left\{ \overline{P_2(\cos\theta) P_2(\cos\beta_r)} - \frac{3}{4} \xi \sin^2\beta_r \, \overline{\sin^2\theta} \right\}$$

$$V_{zz}^m = v_Q^m \left\{ \overline{P_2(\cos\theta) P_2(\cos\beta_m)} - \frac{3}{4} \sin^2\beta_m \, \overline{\sin^2\theta \cos 2\alpha_m} \right.$$

$$\left. + \frac{3}{4} \sin 2\beta_m \, \overline{\sin 2\theta \sin\alpha_m} \right\}$$

$$\bar{V}^r_{xx} - \bar{V}^r_{yy} = \frac{1}{2}\bar{v}^r_Q\{\bar{\eta}^r[1 + \cos^2(\varepsilon + t)] + 3\sin^2(\varepsilon + t)\}$$

$$\cdot \bar{V}^m_{xx} - \bar{V}^m_{yy} = \frac{1}{2}\bar{v}^m_Q\{\bar{\eta}^m[1 + \cos^2\varepsilon] + 3\sin^2\varepsilon\}$$

$$V^r_{xx} - V^r_{yy} = \frac{3}{2}v^r_Q\{-\overline{\sin^2\theta}\, P_2(\cos\beta_r) + \xi \sin\beta^2_r\, \overline{\cos\theta}\}$$

$$V^m_{xx} - V^m_{yy} = \frac{3}{2}v^m_Q\{-\overline{\sin^2\theta}\, P_2(\cos\beta_m) + \sin\beta^2_m\, \overline{\cos\theta\cos 2\alpha_m}$$

$$+ \sin 2\beta_m\, \overline{\sin\theta\sin\alpha_m}\}$$

$$\bar{V}^r_{xz} = \frac{1}{4}\bar{v}^r_Q \sin 2(\varepsilon + t)(3 - \bar{\eta}^r) \quad \bar{V}^m_{xz} = \frac{1}{4}\bar{v}^m_Q \sin 2\varepsilon(3 - \bar{\eta}^m)$$

$$V^r_{yz} = -\frac{3}{4}v^r_Q\{\overline{\sin 2\theta}\, P_2(\cos\beta_r) + \xi \sin\beta^2_r\, \overline{\sin\theta}\}$$

$$V^m_{yz} = -\frac{3}{4}v^m_Q\{\overline{\sin 2\theta}\, P_2c(\cos\beta_m) + \sin^2\beta_m\, \overline{\sin\theta\cos 2\alpha_m}$$

$$- \sin 2\beta_m\, \overline{\cos\theta\sin\alpha_m}\} \tag{14}$$

where: $\overline{f(\theta, \alpha_m)} = Z^{-1}\int_0^\pi f(\theta, \alpha_m)e^{-V_0\cos 2\alpha_m}\, d\alpha_m$; $\theta = \arccos[1 + 2k(1 - \cos 2\alpha_m)]^{-1/2}$; $\xi = \cos 2\alpha_r \cos 2\psi$; Z = normalizing constant and k is a geometrical factor that ensures $\theta = 10.2°$ in the all-trans conformation of the molecular core: $k = \frac{1}{4}[\cos^{-2}(\gamma_0) - 1]$. The angle t is the tilt angle difference between the z axes of the principal frames of the averaged EFG tensors associated with the ring and methine deuterated positions. The angles θ, β_r, β_m and α_m are identified in Figure 3, v^r_Q and v^m_Q were taken as 185 kHz and 177 kHz.[22] The angle γ_0 between the para-axis and the line between the centers of the outer phenyl rings in the all-trans conformation was taken as 10.2°.[25] For β_r and β_m the values 60° and 61.4° were used.[22] From the values of V_0, ξ and ε, one gets finally the order parameters:

$$S^{zz}_{zz} = \frac{\bar{V}^r_{zz}}{V^r_{zz}} = \frac{\bar{V}^m_{zz}}{V^m_{zz}} \quad S^{yz}_{xz} = \frac{3}{4}\frac{\bar{V}^r_{xz}}{V^r_{yz}} = \frac{3}{4}\frac{\bar{V}^m_{xz}}{V^m_{yz}}$$

$$(S^{xx}_{xx} - S^{xx}_{yy}) - (S^{yy}_{xx} - S^{yy}_{yy}) = 3\frac{\bar{V}^r_{xx} - \bar{V}^r_{yy}}{V^r_{xx} - V^r_{yy}} = 3\frac{\bar{V}^m_{xx} - \bar{V}^m_{yy}}{V^m_{xx} - V^m_{yy}} \tag{15}$$

S^{zz}_{zz} gives the order of the long core axis while $(S^{xx}_{xx} - S^{xx}_{yy}) - (S^{yy}_{xx} - S^{yy}_{yy})$ and S^{yz}_{xz} are mainly determined by the biased core rotation around that axis in the herringbone lattice.

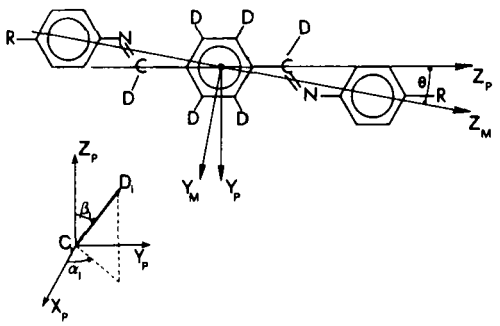

FIGURE 3 Molecular core and different reference frames used. The (X_P, Y_P, Z_P) frame is defined with the Z_P axis parallel to the para-axis and the Y_P axis in the plane of the molecule in the all-trans conformation. The (X_M, Y_M, Z_M) is the principal molecular core frame.

III. EXPERIMENTAL DETAILS

We present a study performed on three liquid crystalline mixtures of protonated and selectively deuterated compounds depicted below that exhibit wide temperature range S_F phases: terephthal-bis-*n*-octylaniline (TBOA) + terephthal-bis-*n*-butylaniline (4 deuterons in the central ring plus 2 deuterons in the linkage groups) (TBBA-d_6) with a 50% to 50% concentration ratio by weight, terephthal-bis-*n*-octylaniline α-d_4 (TBOAα-d_4) + terephthal-bis-*n*-butylaniline (TBBA) with a 50% to 50% concentration ratio by weight and terephthal-bis-*n*-decylaniline (TBDA) + terephthal-bis-*n*-butylaniline (4 deuterons in the central ring plus deuterons in the linkage groups) (TBBA-d_6) with a 25% to 75% concentration ratio by weight.

TBOA $C_8H_{17} - \Phi - N = CH - \Phi - CH = N - \Phi - C_8H_{17}$

TBOα-d_4 $C_7H_{15}CD_2 - \Phi - N = CH - \Phi - CH = N - \Phi - CD_2C_7H_{15}$

TBDA $C_{10}H_{21} - \Phi - N = CH - \Phi - CH = N - \Phi - C_{10}H_{21}$

TBBA-d_6 $C_4H_9 - \Phi - N = CD - \Phi - CD = N - \Phi - C_4H_9$

D_4

The transition temperatures for the different mixtures are:

TBOA + TBBA-d_6

$S_G \underset{\leftarrow}{121} S_F \underset{\leftarrow}{143} S_C \underset{\leftarrow}{161} S_A \underset{\leftarrow}{209} N \underset{\leftarrow}{216} I$

TBOAα-d_4 + TBBA

$S_G \underset{\leftarrow}{120} S_F \underset{\leftarrow}{144} S_C \underset{\leftarrow}{163} S_A \underset{\leftarrow}{209} N \underset{\leftarrow}{216} I$

TBDA + TBBA-d_6

$S_G \underset{\leftarrow}{108} S_F \underset{\leftarrow}{148} S_C \underset{\leftarrow}{178} S_A \underset{\leftarrow}{201} I$

The compounds used were synthesized by the Kent State LCI synthesis group.[26] Both powder and aligned samples of the mixtures studied were prepared. The powder samples were obtained by raising the sample temperature to the isotropic phase and then by cooling it relatively fast outside the magnetic field. The data were recorded going up in temperature. The aligned samples were prepared by raising the sample temperature to the isotropic phase in the presence of a 4.7 T magnetic field, followed by a slow cooling to the S_A phase where the sample was rotated about an axis perpendicular to the magnetic field by about 20°. This rotation was made to help to relieve elastic distortions in the S_C phase and to break the degeneracy in the tilt direction creating a monodomain. The sample was then cooled to a temperature well into the S_G phase. The data were recorded going up in temperature. For each temperature 20 spectra for different values of θ_0 were recorded. The orientation of the sample about an axis perpendicular to the magnetic field was set by a computer controlled step motor with a minimum step in θ_0 of 0.05°.

The deuterium NMR experiments were performed at 30.8 MHz using a Nalorac superconducting magnet and a home-build coherent pulsed spectrometer with quadrature detection interfaced through a Biomation 2805 digitizer to a Digital Equipment Corporation LSI-11/73 computer. The spectra were obtained using a quadrupolar echo sequence $(\pi/2 - \tau - \pi/2 - \tau - \text{acq})$[27] with appropriate phase cycling. τ was 100 μs and the length of the $\pi/2$ pulse was 5 μs. The digitized free induction decay with a length of $2k$ points ($k = 1024$) was average between 1000 and 2500 times according to the signal-to-noise ratio. The complex Fourier transform was performed over $4k$ points per channel by zero filling the additional $2k$ points. The sample temperature was regulated by a circulating fluid provided by a Neslab high temperature thermal bath with a resolution of 0.1°C and a stability in the sample of the same value. The sample temperature was measured by a platinum resistor placed in the sample chamber and connected to a resistance measuring device.

IV. RESULTS

A. Powder Sample Data

Spectra from the powder samples of the three mixtures were recorded spanning all the smectic phases. Typical spectra of each phase for each mixture are shown in Figures 4, 5 and 6. From the simulation of powder spectra in the S_F and S_G phases using Equation (4) the values of $\bar{\nu}_Q$ and $\bar{\eta}$ for all deuterated sites were obtained as a function of temperature and are shown in Figures 7 and 8. Typical simulations are shown in Figure 9. Spectra in the S_F phase very near the S_F-S_C phase transition begin to show some distortion but the values of $\bar{\nu}_Q$ and $\bar{\eta}$ can still be accurately measured even near the transition. Increasing spectral distortion in the proximity of the S_F-S_C phase transition can be attributed to a partial reorientation of the molecules inside each domain as happens in the monodomain sample.

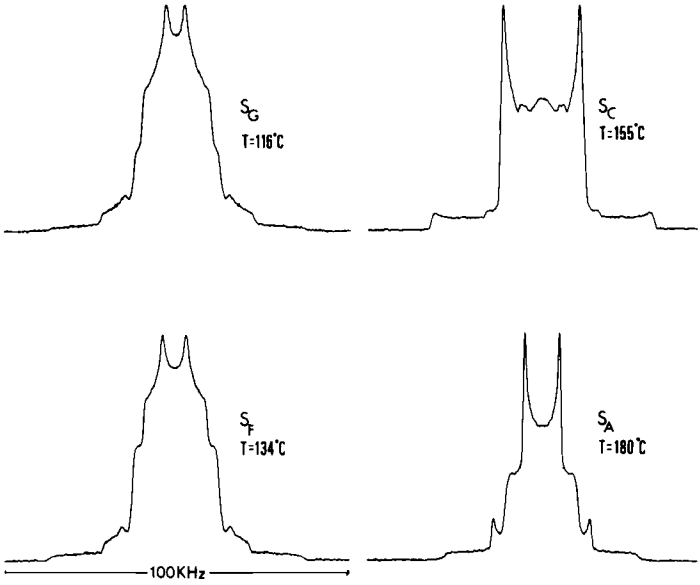

FIGURE 4 Typical spectra obtained in the different mesophases of the mixture TBOA + TBBA-d_6. The spectra were obtained starting with a polycrystalline sample and heating to the desired temperatures in the mesophases indicated.

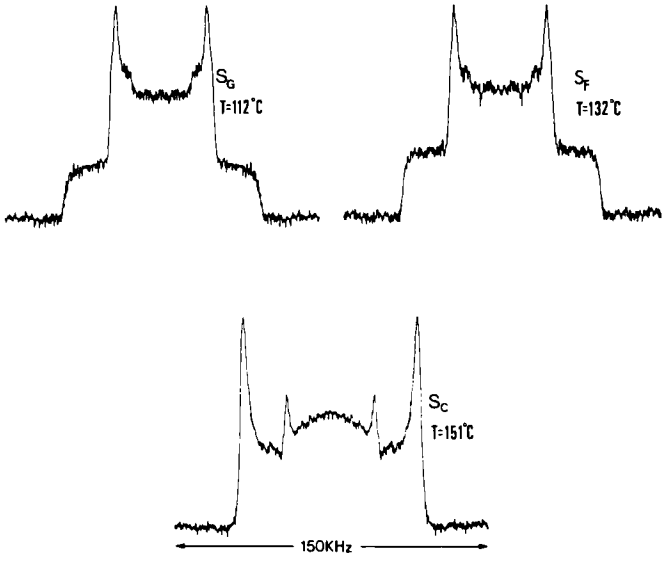

FIGURE 5 Typical spectra obtained in the different mesophases of the mixture TBOAα-d_4 + TBBA. The spectra were obtained starting with a polycrystalline sample and heating to the desired temperatures in the mesophases indicated.

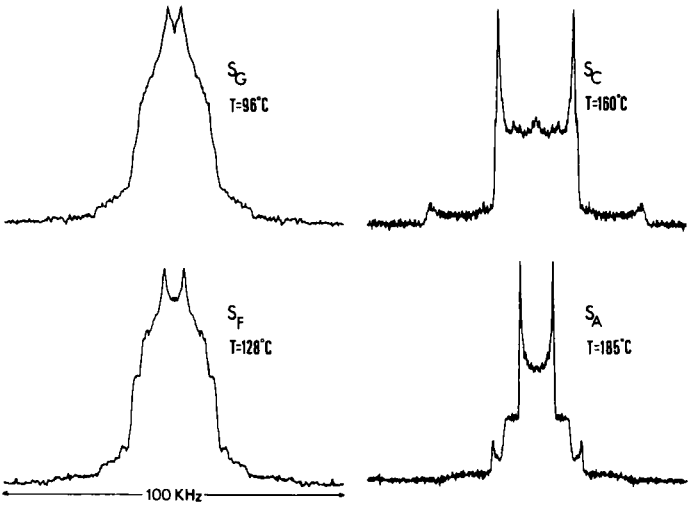

FIGURE 6 Typical spectra obtained in the different mesophases of the mixture TBDA + TBBA-d_6. The spectra were obtained starting with a polycrystalline sample and heating to the desired temperatures in the mesophases indicated.

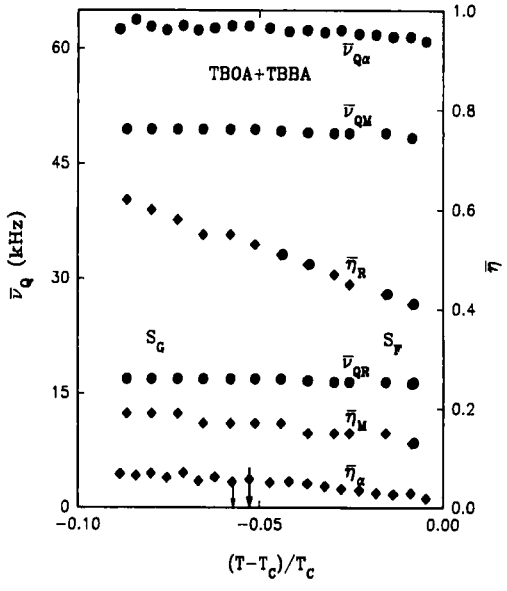

FIGURE 7 Temperature dependence of $\bar{\nu}$ and $\bar{\eta}$ from the central ring (R), and methine (M) and alpha (α) deuterated positions in the mixtures TBOA + TBBA-d_6 and TBOAα-d_4 + TBBA. T_C is the S_F-S_C transition temperature. The larger arrow indicates the S_G-S_F transition temperature for the mixture TBOA + TBBA-d_6. The smaller arrow indicates the S_G-S_F transition temperature for the mixture TBOAα-d_4 + TBBA.

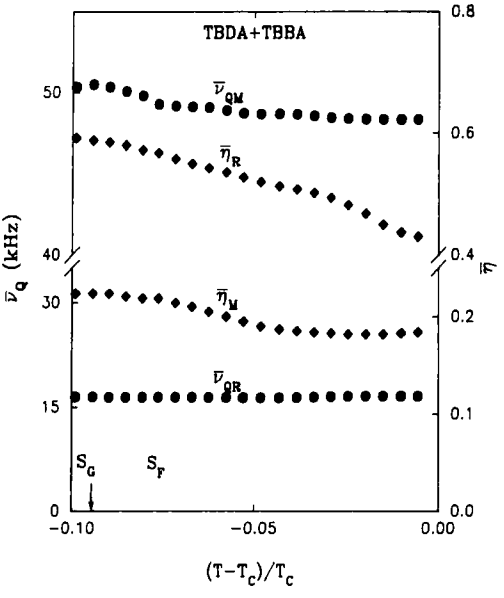

FIGURE 8 Temperature dependence of $\bar{\nu}_Q$ and $\bar{\eta}$ from the central ring (R) and methine (M) deuterated positions in the mixture TBDA + TBBA-d_6. T_C is the S_F-S_C transition temperature. The arrow indicates the S_G-S_F transition temperature.

The spectra in the S_C phase do not correspond to spectra of a spherically distributed powder sample, and cannot be simulated by Equation (4). Assuming that the molecules in the S_C phase reorient completely inside each domain but the domain orientation is still random, the spectra in the S_C phase is simulated as shown in Figure 10. The domain orientation must still be random in the S_C phase so that a uniaxial powder pattern is obtained when the S_A phase is reached as experimentally verified (Figures 4 and 6). The simulation of the S_C powder pattern is not sensitive to the value of $\bar{\eta}$ preventing its determination in this phase.

B. Aligned Sample Data

Analyses of the powder sample data yielded the principal values of the averaged EFG tensors. To obtain the orientations of the principal axes of the averaged EFG tensors in the smectic layers we must use aligned (monodomain) samples. Spectra from the monodomain samples with deuterations in the molecular core were recorded for 20 values of the angle θ_0 at each temperature and for several temperatures spanning both the S_G and S_F phases. In the S_C phase this technique could not be applied because the smectic layers distort under sample reorientation. In the S_G phase the spectra are constituted by two relatively sharp lines for each non-equivalent deuterated position. Fitting the angular dependence of the quadrupolar splitting from each deuterated site with Equation (5) as is shown in Figure 11 allows the values of $\bar{\nu}_Q$, $\bar{\eta}$ and tilt angle θ to be obtained for each non-equivalent deuterated position. The angular dependence of the quadrupolar splittings in the S_F phase is shown in Figure 12. Two new features are present relative to the equivalent data in the S_G phase: the first point is the discontinuity in the splitting for $\theta_0 = 100°$

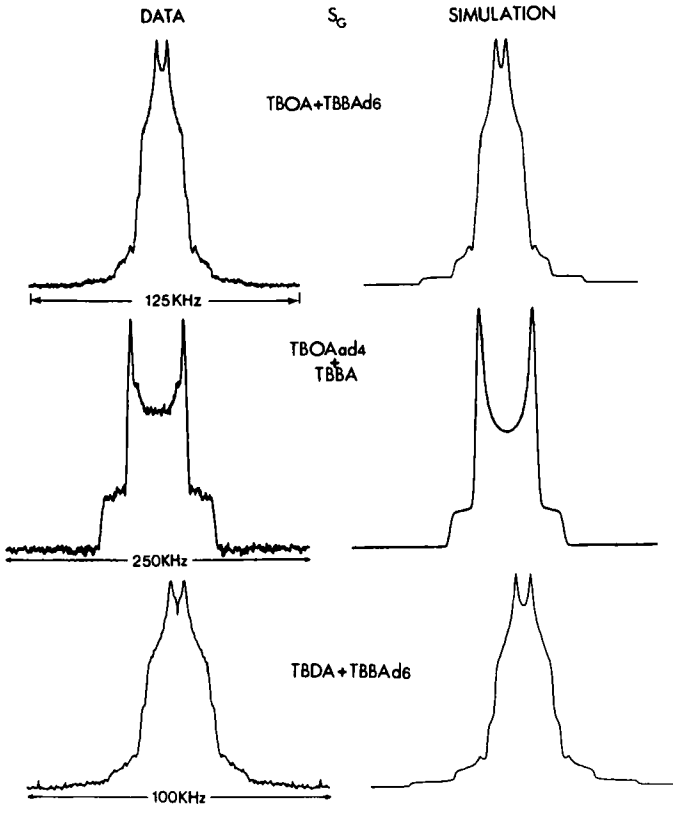

FIGURE 9 Typical spectra from the three mixtures in the S_G phase and theoretical simulations. The spectra were obtained starting with a polycrystalline sample and heating to the desired temperatures.

and the discontinuity in slope for $\theta_0 = 0°$ and $\theta_0 = 180°$. This can be explained considering that in the S_F phase the molecules are seen to change their tilt direction in order to be as parallel as possible to the magnetic field.[14] This change in tilt direction is incorporated in Equation (5) when the data from the S_F is fitted. The second point regards the appearance of a doublet in each spectral line for values of θ_0 near 0° and 180°. A model to explain these doublets in the S_F phase was proposed in a earlier work.[14] The values of $\bar{\nu}_Q$, $\bar{\eta}$ and tilt angle θ were obtained by fitting Equation (5) to the angular dependence of the quadrupolar splittings with the anomalous splittings removed. The values thus obtained for $\bar{\nu}_Q$ and $\bar{\eta}$ are within experimental error identical to those obtained with powder samples. The temperature dependence of the tilt angles from the methine and ring sites is shown in Figures 13 and 14. The discrepancy between the S_F-S_G phase transition temperatures in the sample TBOA + TBBA-d_6 from the powder sample and aligned sample studies is due to some degradation that occurred during the time consuming aligned sample study.

The monodomain sample study shows that in the S_F and S_G phases the ring interactions and the methine interactions do not share the same principal axes, the same holds also for the alpha position (data not reported here).

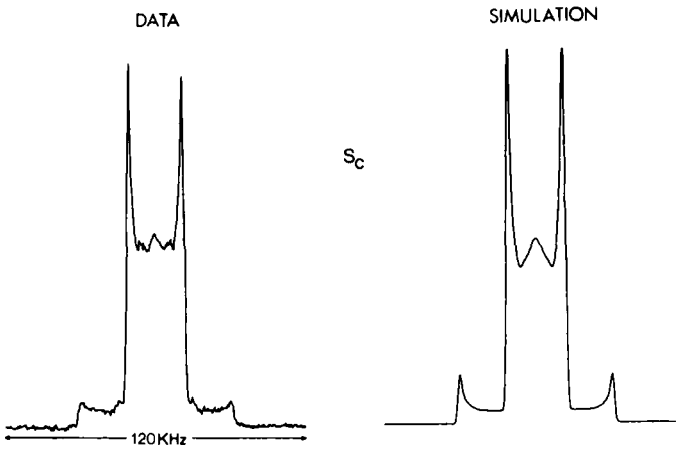

FIGURE 10 Typical spectrum in the S_C phase from the mixtures with deuterations in the molecular core and theoretical simulation. The experimental spectrum was obtained starting with a polycrystalline sample and raising the temperature to the S_C phase. The simulation was carried out assuming a random distribution of domains in the sample and allowing the molecules in each domain to reorient in the tilt cone minimizing their magnetic energy.

V. DISCUSSION

A. Values Obtained for $\tilde{v}_Q$, $\tilde{\eta}$ and θ

The first relevant feature is that the averaged EFG tensors from different sites have distinct principal axes frames and show different asymmetry parameters. At the chain position the asymmetry is very small pointing the absence of in-plane order while the central ring positions show a high asymmetry implying a strong in-plane order. This observation is in agreement with the x-ray studies by F. Moussa *et al.*[10] in the S_F phase reporting the presence of two sub-layers, one formed by the aliphatic chains with liquid like correlations between them and the other formed by the aromatic cores responsible for the molecular order. The second point to notice is that there are no discontinuities at the S_G-S_F phase transition in the measured quantities. It is known from x-ray work[28] that local herringbone order is present in the S_G phase. Since the asymmetry in the averaged EFG tensor is very sensitive to the presence of this type of order,[29] one must conclude that local-herringbone order is also present in the S_F phase.

B. Core Order Parameters in TBOA + TBBA-d_6

The values of the fitting parameters V_0, ξ and ε are shown in Table I. The order parameters are given as a function of temperature in Figure 15. The temperature dependence of V_0, implies for the hindering potential a height of 15 kJ/mole. The angle θ has a value around 9.4° in the temperature range analyzed. The values obtained for the angle ε indicate that the average orientation of long molecular axis coincides with the z axis of the principal frame of the averaged field gradient tensor from the methine-deuteriums. The quantity $\overline{\cos 2\alpha_m}$ describes the bipolar order of the methine deuteriums, it is found to be about -0.74. The values of the

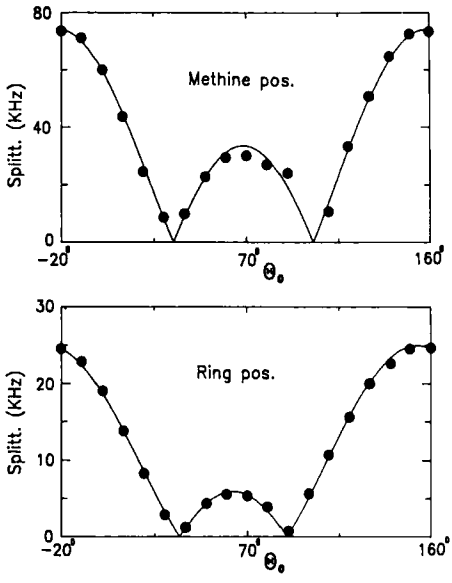

FIGURE 11 Typical angular dependence of the quadrupolar splitting from the ring and methine sites in a monodomain sample of the mixtures TBOA + TBBA-d_6 and TBDA + TBBA-d_6 in the S_G phase. Similar angular dependencies were obtained at the different temperatures analyzed in this phase. The solid line is a fit with Equation (5) allowing the determination of $\bar{\nu}_Q$, $\bar{\eta}$ and θ.

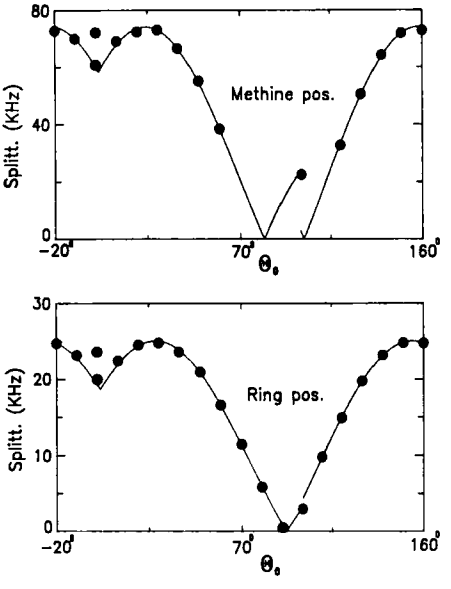

FIGURE 12 Typical angular dependence of the quadrupolar splitting from the ring and methine sites in a monodomain sample of the mixtures TBOA + TBBA-d_6 and TBDA + TBBA-d_6 in the S_F phase. Similar angular dependencies were obtained at the different temperatures analyzed in this phase. The solid line is a fit with Equation (5) allowing the determination of $\bar{\nu}_Q$, $\bar{\eta}$ and θ.

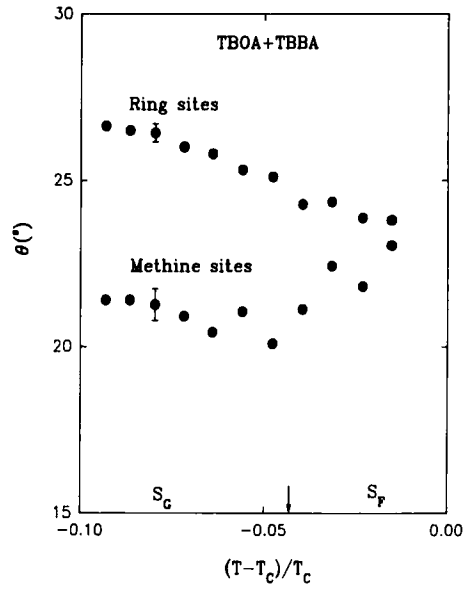

FIGURE 13 Temperature dependence of the tilt angle from the ring and methine deuterated sites in the mixture TBOA + TBBA-d_6, obtained from a monodomain sample angular dependence study. T_C is the S_F-S_C transition temperature. The arrow indicates the S_G-S_F transition temperature.

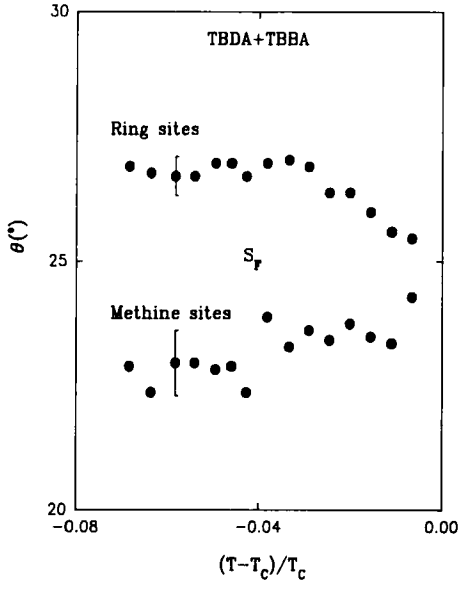

FIGURE 14 Temperature dependence of the tilt angle from the ring and the methine deuterated sites in the mixture TBDA + TBBA-d_6, obtained from a monodomain sample angular dependence study. T_C is the S_F-S_C transition temperature.

TABLE I

Temperature dependence of the fitting parameters in the proposed model for the mixture TBOA + TBBA-d_6. T_C is the S_F-S_C transition temperature

$\frac{T-T_C}{T_C}$	$V_0 \pm \Delta V_0$		$\varepsilon \pm \Delta\varepsilon$ (°)		$\xi \pm \Delta\xi$	
-0.0867	2.33	0.18	0.0	0.5	-0.987	0.042
-0.0798	2.34	0.18	-0.1	0.5	-0.958	0.041
-0.0726	2.34	0.18	-0.1	0.5	-0.927	0.041
-0.0655	2.31	0.19	-0.1	0.5	-0.976	0.046
-0.0581	2.30	0.19	-0.1	0.5	-0.975	0.046
-0.0512	2.31	0.19	-0.1	0.5	-0.942	0.045
-0.0441	2.32	0.19	-0.1	0.5	-0.914	0.044
-0.0369	2.29	0.21	0.0	0.5	-0.986	0.051
-0.0297	2.31	0.21	-0.1	0.5	-0.942	0.049
-0.0255	2.32	0.21	-0.1	0.5	-0.906	0.048
-0.0155	2.33	0.21	0.0	0.5	-0.868	0.047
-0.0085	2.28	0.23	0.0	0.5	-0.948	0.056

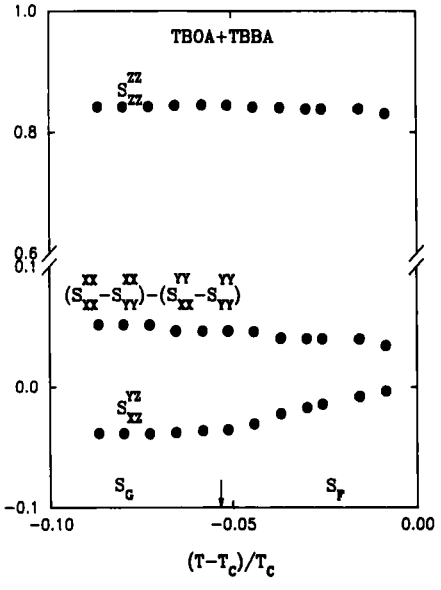

FIGURE 15 Temperature dependence of the order parameters S_{zz}^{zz}, $(S_{xx}^{xx} - S_{yy}^{xx}) - (S_{xx}^{yy} - S_{yy}^{yy})$ and S_{xz}^{yz} in the mixture TBOA + TBBA-d_6. T_C is the S_F-S_C transition temperature. The arrow indicates the S_G-S_F transition temperature.

TABLE II

Temperature dependence of the fitting parameters in the proposed model for the mixture TBDA + TBBA-d_6. T_C is the S_F-S_C transition temperature

$\frac{T-T_C}{T_C}$	$V_0 \pm \Delta V_0$	$\varepsilon \pm \Delta\varepsilon$ (°)	$\xi \pm \Delta\xi$
-0.0714	2.38 0.18	-0.2 0.5	-0.786 0.033
-0.0668	2.38 0.18	-0.2 0.5	-0.788 0.034
-0.0622	2.37 0.18	-0.2 0.5	-0.797 0.035
-0.0574	2.36 0.18	-0.2 0.5	-0.807 0.035
-0.0529	2.35 0.18	-0.2 0.5	-0.816 0.036
-0.0482	2.34 0.18	-0.2 0.5	-0.822 0.037
-0.0432	2.34 0.18	-0.2 0.5	-0.822 0.038
-0.0384	2.33 0.18	-0.2 0.5	-0.827 0.038
-0.0337	2.32 0.18	-0.2 0.5	-0.825 0.038
-0.029	2.31 0.18	-0.2 0.5	-0.82 0.039
-0.0243	2.3 0.18	-0.2 0.5	-0.807 0.038
-0.0195	2.3 0.18	-0.2 0.5	-0.786 0.038
-0.0148	2.3 0.18	-0.2 0.5	-0.757 0.037
-0.01	2.31 0.18	-0.2 0.5	-0.734 0.036
-0.0055	2.3 0.182	-0.1 0.5	-0.72 0.035

quantity ξ are around -0.9, indicating that the central ring motions are mostly π flips and the plane of the ring is almost parallel to the Y_P, Z_P plane. Comparing the value of ξ with $\overline{\cos 2\alpha_m}$, we can see that the methine deuteriums show a smaller "internal" order than the central ring deuteriums, implying that the herringbone ordering is most strongly felt at the benzene-ring level.

C. Core Order Parameters in TBDA + TBBA-d_6

The values of the fitting parameters V_0, ξ and ε are shown in Table II. The order parameters are given as a function of temperature in Figure 16. The temperature dependence of V_0, implies for the hindering potential a height of 16 kJ/mole. For the quantities θ, $\overline{\cos(2\alpha_m)}$ and ε similar values to those obtained with TBOA were found. The quantity ξ is, on the average, smaller than the values found in the mixture TBOA + TBBA, this may indicate either a different average orientation of the central ring in the molecular frame or a decrease of its internal order or both, as ξ is a product of a dynamical quantity and an orientation dependent quantity. Nevertheless it is more likely that the smaller ξ is due to a different average orientation of the central ring.

It is seen in both mixtures that while the long axis order S_{zz}^{zz} is almost temperature independent in the temperature range studied, the bipolar order $(S_{xx}^{xx} - S_{yy}^{xx}) - (S_{xx}^{yy} - S_{yy}^{yy})$ and S_{xz}^{yz} decrease significantly when approaching the S_F-S_C phase tran-

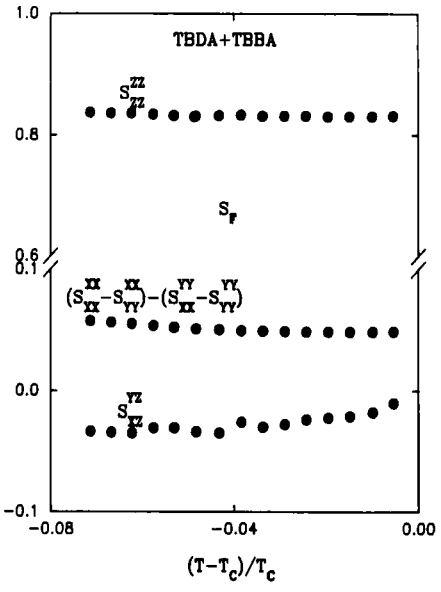

FIGURE 16 Temperature dependence of the order parameters S_{zz}^{zz}, $(S_{xx}^{xx} - S_{yy}^{xx}) - (S_{xx}^{yy} - S_{yy}^{yy})$ and S_{xz}^{yz} for the mixture TBDA + TBBA-d_6. T_C is the S_F-S_C transition temperature.

sition. The behavior of S_{xz}^{yz} near the S_F-S_C transition points for a very small or null value of this order parameter in the S_C phase. A zero value for S_{xz}^{yz} implies that the different interactions of the molecular core share the same principal axes. The x-ray studies of Brock *et al.*[30] suggesting the possible existence of weak herringbone order in the S_C phase favor a small but finite value of S_{xz}^{yz} in this phase.

VI. CONCLUSIONS

This study shows that orientational order in the S_F and S_G phases is very similar. This confirms the existence of local herringbone order in the S_F phase first seen in a earlier work on the compound 90.4.[14] It was also found that the different quadrupolar interactions analyzed in the molecule do not share the same principal axes as allowed by the C_{2h} symmetry of these phases.[17] Quantitative analysis showed that the long axis order is weakly temperature dependent in the range studied, and has a value around 0.82, while the bipolar order and S_{xz}^{yz} decrease significantly when approaching the S_F-S_C phase transition. Across the S_G-S_F phase transition no noticeable variations in the molecular orientational order are observed, showing that orientational order does not play a significant role in this transition. Decrease of bipolar order and S_{xz}^{yz} when approaching the S_F-S_C transition from below, shows progressive loss of in-plane structure and can be explained by the progressive isotropization of the motion around the long molecular axis with the approach of the S_C phase.

Acknowledgment

The authors thank the referee for his helpful remarks and acknowledge the support of the National Science Foundation under the Solid State Chemistry grant No. DMR 91-20130.

References

1. D. Demus, S. Diele, M. Klapperstuck, V. Link and H. Zaschke, *Mol. Cryst. Liq. Cryst.*, **15**, 161 (1971).
2. A. J. Leadbetter, J. P. Gaughan, B. Kelly, G. W. Gray and J. Goodby, *J. Phys. C*, **40**, 178 (1979).
3. J. J. Benattar, J. Doucet, M. Lambert and A. M. Levelut, *Phys. Rev. A*, **20**, 2505 (1979).
4. J. W. Goodby, G. W. Gray, A. J. Leadbetter and M. A. Mazid, in *Liquid Crystals of One- and Two-Dimensional Order*, edited by W. Helfrich and G. Heppke (Springer-Verlag, Berlin, 1980).
5. S. Kumar, *Phys. Rev. A*, **23**, 3207 (1981).
6. P. A. C. Gane, A. J. Leadbetter and P. G. Wrighton, *Mol. Cryst. Liq. Cryst.*, **66**, 247 (1981).
7. P. A. C. Gane, A. J. Leadbetter, J. J. Benattar, F. Moussa and M. Lambert, *Phys. Rev. A*, **24**, 2694 (1981).
8. S. Kumar, *J. Phys.*, **44**, 123 (1983).
9. J. J. Benattar, F. Moussa and M. Lambert, *J. Chim. Phys.*, **80**, 1 (1983).
10. F. Moussa, J. J. Benattar and C. Williams, *Mol. Cryst. Liq. Cryst.*, **99**, 145 (1983).
11. R. J. Birgeneau and J. D. Litster, *J. Phys. Lett.*, **39**, 399 (1978).
12. B. Halperin and D. Nelson, *Phys. Rev. Lett.*, **41**, 121 (1978).
13. J. J. Benattar, B. Deloche and J. Charvolin, *J. Phys.*, **46**, 2179 (1985).
14. J. Figueirinhas, S. Zumer and J. W. Doane, *Phys. Rev. A*, **35**, 4389 (1987).
15. R. Bruinsma and G. Aeppli, *Phys. Rev. Lett.*, **48**, 1625 (1982).
16. A. Abragam, *The Principles of Nuclear Magnetism*, (Oxford University Press, Oxford England, 1961).
17. J. C. Toledano and P. Toledano, *The Landau Theory of Phase Transitions* (World Scientific Publishing, USA 1987).
18. J. Seliger, R. Osredkar, V. Zagar and R. Blinc, *Phys. Rev. Lett.*, **38**, 411 (1977).
19. J. Seliger, V. Zagar and R. Blinc, *Phys. Rev. A*, **17**, 1149 (1978).
20. A. J. Dianoux and F. Volino, *J. Phys.*, **40**, 181 (1979).
21. R. Blinc, J. Seliger, M. Vilfan and V. Zagar, *J. Chem. Phys.*, **70**, 778 (1979).
21. A. J. Dianoux and F. Volino, *J. Phys.*, **41**, 1147 (1980).
23. F. Volino, A. J. Dianoux, J. Berges and H. Perrin, *Mol. Cryst. Liq. Cryst.*, **90**, 281 (1983).
24. C. Zannoni in *Nuclear Magnetic Resonance of Liquid Crystals*, edited by J. W. Emsley (NATO ASI Series, Serie C, 1983).
25. Z. Luz, R. C. Hewitt and S. Meiboom, *J. Chem. Phys.*, **61**, 1758 (1974).
26. M. E. Neubert, *Mol. Cryst. Liq. Cryst.*, **129**, 327 (1985).
27. J. H. Davis, K. R. Jeffrey, M. Bloom, M. I. Valic and T. P. Higgs, *Chem. Phys. Lett.*, **42**, 390 (1976).
28. A. M. Levelut, *J. Phys.*, **37**, C51 (1976).
29. N. A. Vaz, M. J. Vaz and J. W. Doane, *Phys. Rev. A*, **30**, 1008 (1984).
30. J. D. Brock, A. Aharony, R. J. Birgeneau, K. W. Evans-Lutterodt, J. D. Litster, P. M. Horn, G. B. Stephenson and A. R. Tajbakhsh, *Phys. Rev. Lett.*, **57**, 98 (1986).